

Contract No:

This document was prepared in conjunction with work accomplished under Contract No. DE-AC09-08SR22470 with the U.S. Department of Energy (DOE) Office of Environmental Management (EM).

Disclaimer:

This work was prepared under an agreement with and funded by the U.S. Government. Neither the U. S. Government or its employees, nor any of its contractors, subcontractors or their employees, makes any express or implied:

- 1) warranty or assumes any legal liability for the accuracy, completeness, or for the use or results of such use of any information, product, or process disclosed; or
- 2) representation that such use or results of such use would not infringe privately owned rights; or
- 3) endorsement or recommendation of any specifically identified commercial product, process, or service.

Any views and opinions of authors expressed in this work do not necessarily state or reflect those of the United States Government, or its contractors, or subcontractors.



L Basin Corrosion Surveillance Program – Evaluation of 2014 Surveillance Coupons

J.I. Mickalonis

T. H. Murphy

December 2017

SRNL-TR-2017-00415, Revision 0



DISCLAIMER

This work was prepared under an agreement with and funded by the U.S. Government. Neither the U.S. Government or its employees, nor any of its contractors, subcontractors or their employees, makes any express or implied:

1. warranty or assumes any legal liability for the accuracy, completeness, or for the use or results of such use of any information, product, or process disclosed; or
2. representation that such use or results of such use would not infringe privately owned rights; or
3. endorsement or recommendation of any specifically identified commercial product, process, or service.

Any views and opinions of authors expressed in this work do not necessarily state or reflect those of the United States Government, or its contractors, or subcontractors.

Printed in the United States of America

**Prepared for
U.S. Department of Energy**

Keywords: *Spent fuel storage, aluminum alloys, pitting corrosion*

Retention: *Permanent*

L Basin Corrosion Surveillance Program – Evaluation of 2014 Surveillance Coupons

J.I. Mickalonis
T. H. Murphy

December 2017

Prepared in conjunction with work accomplished under contract number DE-AC09-08SR22470 with the U.S. Department of Energy (DOE) Office of Environmental Management (EM).



ACKNOWLEDGEMENTS

The authors wish to acknowledge the following for their assistance: H. Ajo, S. Harris, K. Kalbaugh and D. Missimer. The authors are especially indebted to M. Tosten for his diligence in making the pit depth measurements with the laser confocal microscope and developing the new protocol for coupon examination followed in this current analysis.

EXECUTIVE SUMMARY

The L Basin Corrosion Surveillance Program is performed in conjunction with the Spent Fuel Storage Basin Water Chemistry Control Program to evaluate the corrosion of aluminum coupons as an indicator of the degradation of the aluminum-clad spent nuclear fuel stored in L Basin. The latest set of coupons were removed in 2014 after 15 years of exposure. The water quality throughout the exposure period has been within the parameter limits established for basin operation that are consistent with international guidelines for aluminum fuel storage. The 2014 corrosion characterization utilized a new protocol involving a laser confocal microscope for improved characterization of pitting corrosion. This report trends these results with those of previous coupons (2005 – 2010), which were placed in L Basin in 1999.

Pit Characterization Protocol

The characterization of pitting corrosion follows the ASTM International standard guide G46 and includes the determination of pitting parameters, primarily a maximum pit depth and an average of the ten deepest pits. Two measuring systems have been used to measure pit depths, historically a light measuring microscope and more recently a laser confocal microscope. A comparison was performed of the protocol for the two microscopes. The results were found to be similar although the use of the laser confocal microscope resulted in deeper pit measurements, which is attributed to the improved capability of identifying the bottom of the pit.

Corrosion Characterization of 2014 Surveillance Coupons

The 2014 surveillance coupons had slightly higher pit depths than those measured previously as shown in the table below for the average of the ten deepest pits and the maximum pit depth from the three types of coupons. The historical average was calculated for the rates measured on coupons from 2005-2010.

Coupon Type	2014 Coupon Removal (inch)		Historical Average (inch)	
	Average	Maximum	Average	Maximum
Single	0.0037	0.0172	0.0021	0.005 (2006)
Crevice	0.0027	0.0048	0.0021	0.0046 (2006)
Galvanic	0.011	0.0255	0.0076	0.0348 (2010)

The increases are attributed to two primary factors: the use of the laser confocal microscope which improved the capability of identifying the bottom of a pit and the presence of rust particulate on the surface of the coupons, especially on the single coupons. From a review of previous exposure coupons, the deposition of debris (sand for 2006 coupons and rust particulate for 2014 coupons) lead to increases in pit depth on the aluminum coupons. As shown by the data in the table, the 2014 results continue to demonstrate that galvanic interactions are aggressive accelerators of aluminum corrosion.

Conclusions and Recommendations

The corrosion characterization of the 2014 surveillance coupons along with those performed previously provide a sound basis that the incidence of pitting is not expected to be mitigated by more stringent control of the water quality. The latest results from the L Basin Corrosion Surveillance Program has shown:

- The use of the laser confocal microscope provides improved capabilities for better characterization of the observed corrosion and the microscope will continue to be used for future characterization.
- The deposition of debris on to the aluminum increases the corrosion as measured by the average pit depth of the ten deepest pits and the maximum measured pit depth.
- A review of basin operation is recommended to determine the source of the rust particulate on the 2014 coupons and probable dates of occurrence.
- Further development of the measurement protocol using statistical analysis be undertaken to improve trending of the corrosion data, reduce the time to perform the analysis, and reduce storage capacity of the data.

TABLE OF CONTENTS

LIST OF TABLES	viii
LIST OF FIGURES	ix
LIST OF ABBREVIATIONS.....	x
1.0 Introduction.....	1
2.0 Evaluation Protocol.....	1
2.1 Coupon Description and Handling	1
2.2 Corrosion Characterization.....	2
3.0 L Basin Water Quality	6
4.0 Coupon Evaluation.....	6
4.1 Visual Evaluation	6
4.2 Surface Analysis.....	9
4.3 Impedance Spectroscopy	11
4.4 Pitting Analysis	12
4.4.1 LCM-Light Comparison	12
4.4.2 2014 Single Coupon Pit Analysis	13
4.4.3 2014 Crevice Coupon Pit Analysis.....	17
4.4.4 2014 Galvanic Aluminum Coupon Pit Analysis.....	18
5.0 Discussion.....	19
6.0 Conclusions.....	20
7.0 References.....	21
Appendix A 2014 Surveillance Coupon Numbers and Configurations	A-23
Appendix B 2014 Surveillance Coupon Photographs – Before and After Cleaning	B-25
Appendix C Photographic Comparison of Surveillance Coupons from 2005 to 2014	C-50
Appendix D XRD Scan of 2014 Aluminum Coupon.....	D-54

LIST OF TABLES

Table 2-1. Aluminum Alloys Nominal Composition used for Basin Corrosion Surveillance Coupons.....	1
Table 2-2. Cleaning Steps for 2014 Corrosion Surveillance Coupons	3
Table 4-1. Visual Evaluation Summary of 2014 Surveillance Coupons.....	7
Table 4-2. Elements Identified in Base Metal Alloys and Exposed Coupon Surfaces	10
Table 4-3. Pit Parameters (inch) Determined Using the Light and the Laser Confocal Microscopes	12
Table 4-4. Measured Pit Depth Distribution from Light Microscope (LM) and Laser Confocal Microscope (LCM) Techniques	13
Table 4-5. Pit-Depth (inch) Summary for 2014 Single Coupons.....	14
Table 4-6. Range of Maximum Pit Depths for Surveillance Coupons Removed from L Basin Between 2005 and 2014	16
Table 4-7. Corrosion Surveillance Coupon Exposure Location in L Basin.....	16
Table 4-8. Pit-Depth (inch) and Density Summary for 2014 Crevice Coupons	18
Table 4-9. Pit-Depth (inch) and Density Summary for 2014 Galvanic Coupons	18

LIST OF FIGURES

Figure 2-1. (A) Photograph of a Junior Ray Gun used for exposing surveillance coupons in L Basin; and (B) Location in L Basin of Junior Ray Gun removed in 2014 (red oval; blue ovals and triangles show locations of remaining surveillance and furniture rack coupons, respectively)	2
Figure 2-2. Template showing the laser confocal microscope quadrant scanning for 2014 surveillance coupons	4
Figure 2-3. Data file of one quadrant from 252 individual images for crevice coupon stitched	4
Figure 2-4. Pit measurement for an individual image from single coupon 1100-032, Q1 on the front or numbered side: (A) laser scan image; (B) height scan with profile line through deepest part of pit; and (C) the profile measurement with the pit depth of 196.05 μm shown in the table	5
Figure 3-1. L Basin Water Quality Parameter Trends - Conductivity, pH and Cs-137 activity over the time period of 1999 through 2014	6
Figure 4-1. Photographs of 2014 L Basin surveillance coupons prior to cleaning: (A) single Al1100 coupon with rust-like patina; (B) single Al6061 coupon without rust patina; (C) mating surfaces from Al 6063 crevice couple; and (D) mating surfaces from Al1100 galvanic couple (304L on left, Al1100 on right).	8
Figure 4-2. Photographs of Al6061 galvanic couple with the 304L coupon surface facing upward and the Al6061 coupon surface facing downward	9
Figure 4-3. X-ray diffraction spectra for Al1100 galvanic coupon #026 downward facing coupon after a 15-year exposure in L Basin	10
Figure 4-4. SEM micrographs showing intermetallic and impurity particles in base aluminum alloys: A) Al1100 (sample ground with 600-grit paper); and B) Al6061	10
Figure 4-5. SEM micrographs showing intermetallic and impurity particles in base aluminum alloy Al6063	11
Figure 4-6. Nyquist plots for single coupons of each aluminum alloy, specifically 1100 #032, 6061 #093, and 6063 #123.....	11
Figure 4-7. Plot of mean pit depth ($>25.4 \mu\text{m}$ (1 mil)) and standard deviation for each 2014 surveillance coupon (the solid line indicates the overall average mean for this data set; color indicates the different quarter the pit was located).....	14
Figure 4-8. Trend plot of the maximum and the 10-deepest average pit depths for single surveillance coupon from 2005 to 2014.....	15
Figure 4-9. Trend plot of the maximum and 10-deepest average pit depths for crevice surveillance coupon from 2005 to 2014	17
Figure 4-10. Trend plot of the maximum and average pit depth for galvanic surveillance coupon from 2004 to 2014	19

LIST OF ABBREVIATIONS

C	crevice couple configuration
CSP	Corrosion Surveillance Program
DOE	Department of Energy
EIS	Electrochemical Impedance Spectroscopy
EDS	Energy Dispersive Spectroscopy
G	galvanic couple configuration
HAZ	heat-affected zone
IAEA	International Atomic Energy Association
JRG	Junior Ray Gun
LCM	Laser Confocal Microscope
M&TE	measuring and testing equipment
mpy	mils per year
ND	no data
PTFE	polytetrafluoroethylene
S	single coupon configuration
SEM	scanning electron microscope
SRNL	Savannah River National Laboratory
XRD	X-ray diffraction

1.0 Introduction

The L Basin Corrosion Surveillance Program (CSP) provides for corrosion monitoring of the materials of construction for the aluminum clad fuel and storage racks during the extended storage in the L Basin water environment. Through early detection of aggressive corrosion, corrosion control measures can be modified or initiated, including adjustments to the basin water quality or fuel storage configuration. The CSP monitors corrosion through the use of surrogate coupons, which are periodically removed for destructive evaluation. The CSP follows the guidelines of both ASTM International and the International Atomic Energy Association (IAEA) [1-5].

The surveillance coupons consist of two types: sections of furniture storage rack components (Al6061 and Al6063) and standard disk-shaped coupons with materials of construction of the fuel cladding (Al1100) and the storage racks. The storage racks are used to support and separate fuel element bundles stored in L Basin. The standard coupons are in three configurations: as single coupons, same alloy coupons coupled together to form a crevice, and as a galvanic couple between 304L stainless steel and aluminum alloy coupons. The furniture rack and disk coupons were placed into L Basin at different times. Furniture rack coupons were initially immersed in 1996, while the standard disk coupons were placed in the basin in 1999 and 2000. This report discusses the evaluation of standard disk coupons that were removed in October 2014 after 15.4 years of exposure.

2.0 Evaluation Protocol

The evaluation of the surveillance coupons were conducted following the corrosion surveillance program plan [6]. The specific details of the protocol followed with the 2014 surveillance coupons are described below. These details include the coupon description and handling, the methods used in the pitting characterization, and the analysis of the data.

2.1 Coupon Description and Handling

The coupons were exposed on a test assembly referred to as the Junior Ray Gun (JRG), which consisted of a rod on to which disk-shaped coupons were assembled as shown in Figure 2-1A. The coupons were in three configurations: single (S), paired with a 304L stainless steel coupon (galvanic couple (G)) or paired with another aluminum coupon of the same composition (crevice couple (C)). Coupons or coupon couples were electrically isolated from the support rod and each other with polytetrafluoroethylene (PTFE) washers. The disk-shaped coupons had the following nominal dimensions: 1.25 in OD, 0.375 inch ID, and 0.12 inch thick. Surfaces had a final surface preparation with 600 grit paper. The nominal compositions of the aluminum alloys are given in Table 2-1; the balance of the composition is aluminum. The coupons were procured from Metal Samples, Inc (Munsford, AL).

Table 2-1. Aluminum Alloys Nominal Composition used for Basin Corrosion Surveillance Coupons

Alloy	Elemental Concentration (wt%)				
	Si	Cu	Mg	Cr	Fe
6061	0.6	0.28	1	0.35	-
6063	0.4	-	0.7	0.1	0.35
1100	*	0.05 -0.2	-	-	*

* Si + Fe < 1%

The coupons were exposed in the southeast part of Horizontal Tube Section (shown by red oval in Figure 2-1B) and initially placed in the basin on May 15, 1999 with removal on October 20, 2014, which resulted in an exposure period of 5637 days or approximately 15.4 years. Appendix A contains the coupons position in the JRG, corresponding number, type of configuration, and the analyses performed.

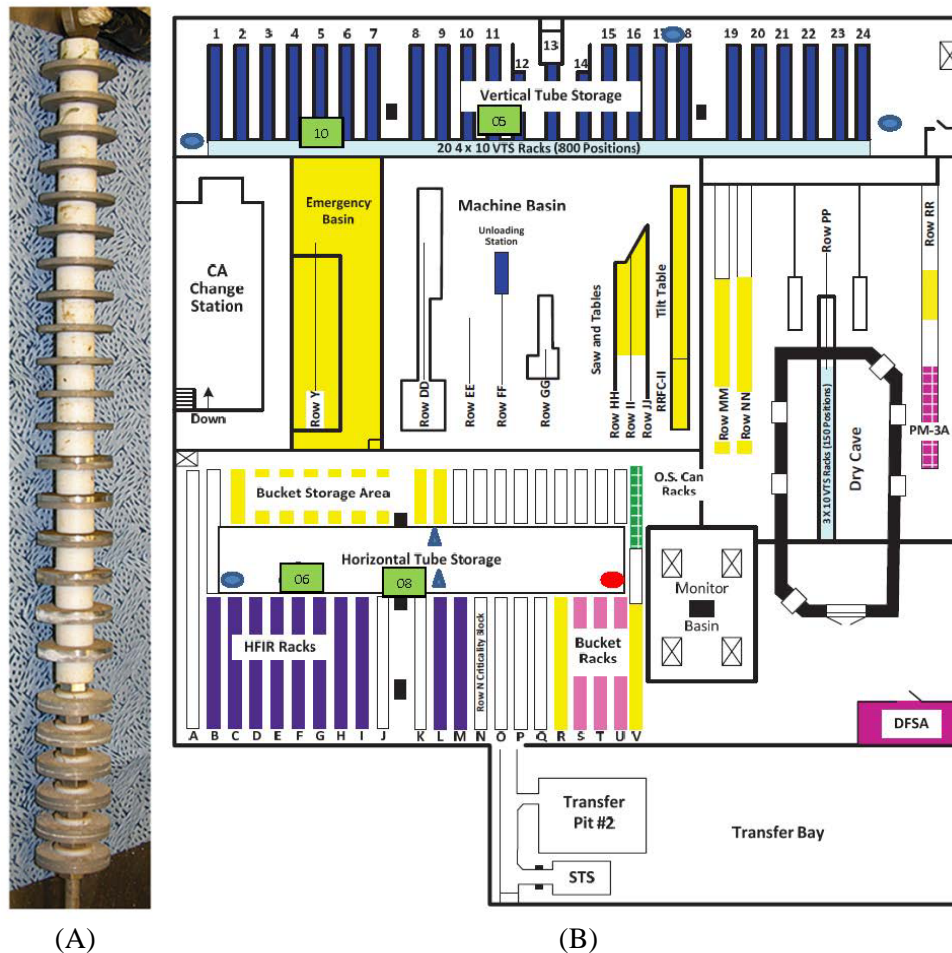


Figure 2-1. (A) Photograph of a Junior Ray Gun used for exposing surveillance coupons in L Basin; and (B) Location in L Basin of Junior Ray Gun removed in 2014 (red oval; blue ovals and triangles show locations of remaining surveillance and furniture rack coupons, respectively)

After the coupons were removed from the basin, the JRG was disassembled and the coupons were placed on a rope in the order taken from the JRG. The coupons did not appear to have sand filter fines on the surface, but they did have a reddish-brown or rust-colored tint [7]. The string of coupons was placed in a carboy with basin water and shipped to SRNL for processing. At SRNL, the coupons were separated by configuration into three bottles containing basin water from the carboy and stored until used for analysis.

2.2 Corrosion Characterization

Both sides of each coupon were photographed in the as-received condition with a digital 35-mm camera. The coupons were photographed wet and immediately put back into storage in the basin water. Prior to cleaning, some coupons were selected for examination by x-ray diffraction (XRD) and scanning electron microscopy (SEM) to characterize the oxide formed during exposure to the basin water as well as electrochemical impedance spectroscopy (EIS) to characterize the relative oxide resistance of each alloy. These coupons are identified in Appendix A. All coupons were cleaned at some point and photographed again. All pre- and post-cleaning photographs of the coupons are shown in Appendix B. After cleaning the coupons were stored in a desiccator until analyzed for pitting.

The EIS characterization of the surface oxide for the selected coupons was performed to determine if the formed oxide was alloy dependent. The different aluminum alloys have different types of inclusion and impurities, which have shown a slight difference in pitting in L Basin water [8, 12-14]. Single coupons were used in the uncleaned condition so that the oxide that formed during exposure in the basin was still intact. Testing was performed with various solutions on an exposed coupon to assess the impact on the impedance spectra since a non-aggressive solution was needed to not alter the oxide as well as with sufficient conductivity to preclude the solution impedance from dominating the spectra. A 1wt% sodium phosphate solution was chosen and testing was conducted at room temperature over a frequency range of 10^{-1} to 10^5 Hz with a perturbation of ± 10 mV. Samples were stabilized in the solution prior to EIS with times varying from an hour to as long as a day until a stable open circuit potential was achieved.

Coupon cleaning was performed in concentrated (16M) nitric acid at room temperature following the guide lines of ASTM International G-1 [4]. The various cleaning steps required for each configuration are shown in Table 2-2. The differences were due to the tenaciousness of the oxide/corrosion products on the coupons. Following each acid soak the coupons were rinsed with distilled water and scrubbed with a soft-bristled brush to remove the oxide prior to examination for pits. During the cleaning, a control coupon was also cleaned to monitor any significant changes in the weight or pitting incidence. As found previously, a new coupon lost on the order of tens of thousandths of a gram (typical coupon weighs ~6 grams) per 10-minute cleaning [8]. Additionally, individual pits from select coupons of each alloy type were measured at different stages during the acid cleaning process with no effect found on pit size (depth and diameter).

Table 2-2. Cleaning Steps for 2014 Corrosion Surveillance Coupons

Coupon Type	Cleaning Time (min)		
	1 st Soak	2 nd Soak*	3 rd Soak*
Single	5	20	
Single - XRD/SEM	15	10	
Galvanic - Al and 304	5	50	
Galvanic – Al, XRD/SEM	15	40	30
Crevice	5	50	30

* Soak performed with ultrasonic agitation.

Laser confocal microscopy was the primary technique used to evaluate the corrosion of the coupons and measure pit depths since it provided improved resolution than a standard light microscope and improved confidence that the true bottom of a pit was identified. A Keyence VK-X110 laser confocal microscope (LCM) with electronic stage was used. Pit depths on select coupons were measured also on a Nikon MM-400 measuring microscope with a Nikon SC3-E1 digital counter (microscope used for 2008, 2010 and 2012 coupons). EMAX software by Excel Technologies was used for data processing of the depth measurements. These Nikon measurements were used to compare data sets with those from the LCM.

The pit depth analysis that has been used since 2004 follows guidelines given in ASTM International G-46 [6]. The primary parameters that have been used to characterize the pitting observed on the surveillance coupons are maximum depth, average depth of the ten deepest pits, and a pit density. The general protocol for obtaining these parameters was to examine the entire coupon measuring pits >0.5 mil since a large pit density below this value was found to exist on coupons removed from the basin. With the LCM, this value was increased to 1 mil since the larger pits are more likely to lead to loss of integrity of the cladding. For the LCM, the variability in a pit depth measurement was ± 2.4 μ m or ± 0.09 mil.

With the Nikon microscope, the protocol was to scan the entire coupon surface at a 100X magnification for identifying pits of large diameter and to measure the pit depth at a 200X magnification. Pit density was calculated for three areas identified as having sufficient and representative pitting at 100X magnification. The magnification was increased to 200X and the number of pits within this view (0.598 mm²) were counted.

For the 2010 surveillance coupons, the pit density was measured for a randomly selected quarter of a coupon side.

For the LCM, both sides of a coupon were scanned in quarter sections as shown by the template in Figure 2-2. Scans were performed with a 10X objective lens. The front or numbered side was scanned first and the template provided the numbering or identification of the quadrants. Each quadrant (16.5 mm x 16.0 mm) consisted of an array of approximately 250 individual images; each quadrant scan took approximately 2.5 hours. Figure 2-3 is a representative raw data file showing the stitched images with optical, laser, laser + optical, and height views.

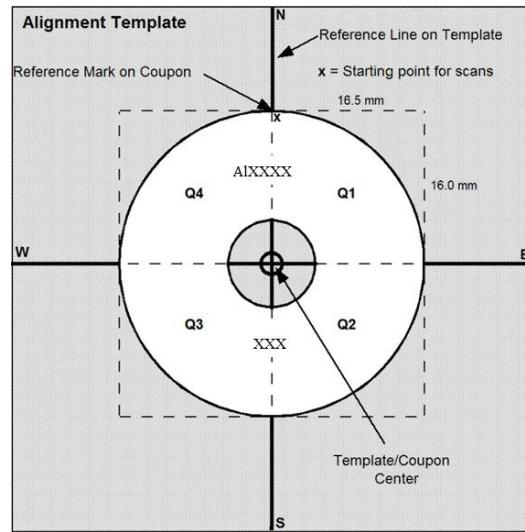


Figure 2-2. Template showing the laser confocal microscope quadrant scanning for 2014 surveillance coupons

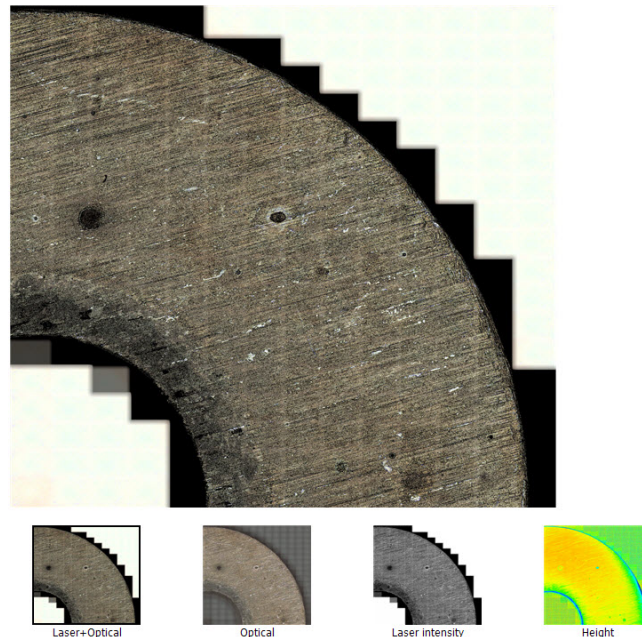


Figure 2-3. Data file of one quadrant from 252 individual images for crevice coupon stitched

For the single coupons, crevice coupons, and the front sides of the Al coupons from the galvanic couples, the resolution of the large stitches was insufficient to pick out individual pits for measurement. The individual images used to compile the large stitches were evaluated singularly to identify deep pits for the depth and diameter measurements. The deep pits were identified visually from the color-coded height scans assigned to an image after each is processed manually for noise reduction and tilt correction. Surface profile measurements, which are performed digitally, were made for the identified pits to determine pit depths. These measurements are demonstrated in Figure 2-4 for the 2014 single coupon 1100-032. In Figure 2-4 (B), the deepest pit was identified by the darkest blue and a profile line placed at a point where the pit was deepest (shown in Figure 2-4 (C)).

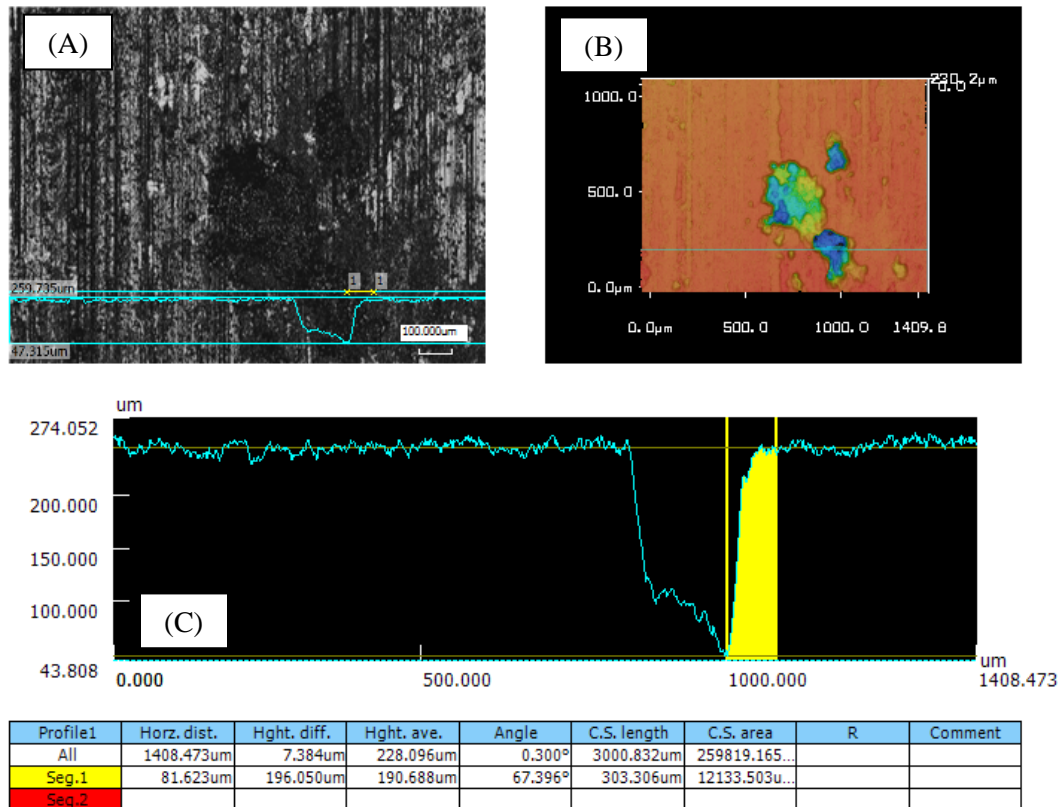


Figure 2-4. Pit measurement for an individual image from single coupon 1100-032, Q1 on the front or numbered side: (A) laser scan image; (B) height scan with profile line through deepest part of pit; and (C) the profile measurement with the pit depth of 196.05 μm shown in the table

Density measurements for each coupon quadrant were made from a 4 X 6 (24 image) subset (approx. 5.1 mm x 5.5 mm region) stitched together from the original set of scanned images, which were obtained with a 10x objective lens. These stitches were processed for noise reduction and tilt correction. Only pits deeper than or equal to 1 mil (approx. 25 μm) were included in the density measurements. The location of the stitched region for pit density measurements varied for front-side quadrants. These locations were chosen to minimize any effect associated with the spacer washer or the identification number stamps. Back-side quadrants were all taken at identical areas within the stitch. Once these locations were chosen for each quadrant, they were used repeatedly on all coupons.

The CSP data for both surveillance and furniture rack coupons (2003-2014) are compiled at \\hpcfs2\hpc_project\projwork8\Mat_tech\L Basin Corrosion. Due to the volume of LCM data from the

2014 surveillance coupons, these data are stored on an external hard drive (currently located in 773-A, D1122). All retained coupons (2004-2014) are currently archived in 773-A, C115.

3.0 L Basin Water Quality

The L Basin water quality has been well controlled over the 2014 surveillance coupons exposure. The L Basin Water Chemistry Control Program establishes limits for the basin water activity and minimizing corrosion of the fuels, bundles, and associated handling and storage equipment. The pH and conductivity limits are: $5.5 \leq \text{pH} \leq 8.5$ and conductivity $< 10 \mu\text{S/cm}$ [16]. The basin water pH and conductivity was maintained within these limits over the time period of May 1999 to October 2014, which are shown in Figure 3-1 along with the Cs-137 activity. The dashed line indicates the date (July 2014) of the discharge of sand filter fines into the basin. The spikes in conductivity and Cs-137 activity correspond to the addition of fuels to the basin as well as operational activities such as maintenance to a deionizer valve and a change in the building air conditioning. The Cs-137 limit, which was established at $< 500 \text{ dpm/ml}$, was exceeded only briefly in 2003 after the addition of failed fuels from RBOF [16]. Chloride concentrations have been consistently below 0.1 ppm.

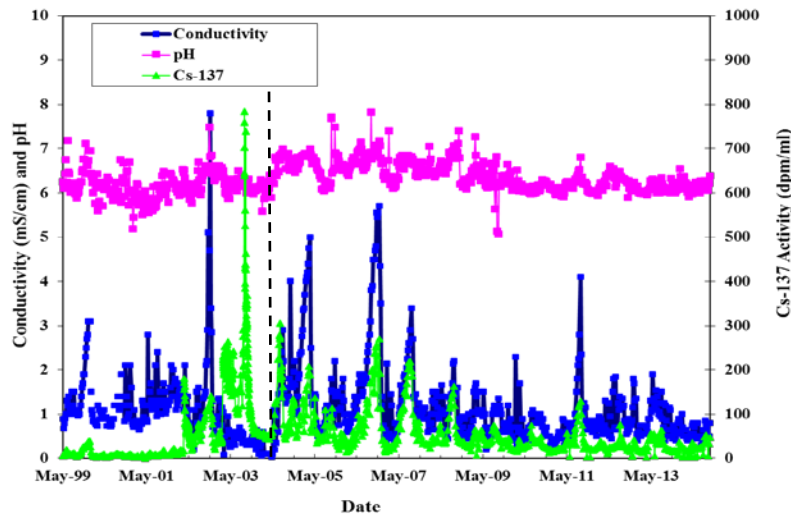


Figure 3-1. L Basin Water Quality Parameter Trends - Conductivity, pH and Cs-137 activity over the time period of 1999 through 2014

The L Basin water is presently maintained by continuous flow through a mixed cation/anion resin bed. No cooling or chemical additions are used to control water conditions.

4.0 Coupon Evaluation

The analysis of the 2014 surveillance coupon consisted of a visual evaluation to characterize the general corrosion morphology, surface analysis including oxide characterization, and pit depth measurements. These results are discussed herein.

4.1 Visual Evaluation

A visual examination of the coupons was performed to characterize the general corrosion morphology; coupons were photographed in the as-received and post-cleaned condition (See Appendix B). The surveillance coupons had variable surface appearances depending primarily on the coupon configuration (i.e. single, galvanic, and crevice). Table 4-1 provides a summary of the visual observations prior to cleaning. Select photographs are shown in Figure 4-1 to highlight some of the differences in the observed corrosion morphology.

Table 4-1. Visual Evaluation Summary of 2014 Surveillance Coupons

Type*	Alloy	Side**	Description
Single	1100	Up	Sporadic rust spots, halos features, oxide build up near washer edge
		Down	Uniform surface oxide, oxide build up near washer edge
	6061	Up	Brown/rust particles especially near circumference, black oxide spots noted
		Down	Uniform surface oxide with some rust spots
	6063	Up	Rust particles heaviest near edge, black spots and halo features
		Down	Some rust spots, halo features, oxide build up near washer edge
Crevice Couple	1100	Up	Brown/rust particles around washer, oxide build up near washer
		Down	Uniform surface oxide, oxide build up near washer edge
		Mating	Mottled oxide near perimeter, cross hatched appearance near center
	6061	Up	Brown/rust particles around washer, oxide build up near washer edge, some black oxide spots
		Down	Uniform surface oxide, oxide build up near washer edge
		Mating	Mottled oxide near perimeter, cross hatched appearance near center
	6063	Up	One coupon has uniform oxide, the other has brown/rust particles too
		Down	Uniform oxide except one coupon has an area with numerous black oxide spots
		Mating	Uniform oxide except around perimeter where oxide is mottled
Galvanic Couple	1100	Down	Large spots of oxide build up on open surface and beneath washer
		Mating	Mottled oxide
	6061	Down	Uniform oxide, oxide under washer, some rust particles
		Mating	Mottled oxide especially around perimeter
	6063	Down	Spots of oxide build up on open surface, oxide beneath washer
		Mating	Mottled oxide especially around perimeter, one coupon has rust colored area

* Types include single coupons, coupons of similar alloy paired as a crevice couple, and coupons paired with 304L coupons as a galvanic couple; areas near and under the PTFE separation washers are differentiated.

** For single coupons and in galvanic couples, aluminum coupon numbered side was faced down. In crevice couples, one aluminum coupon numbered side was faced up, the other faced down. There were some exceptions (See Appendix B).

The coupon orientation during exposure can be confusing, so prior to the discussion of the visual examination the coupon orientation is explained. Each coupon had a unique number and the alloy type engraved on one side, which is referred to in this report as the front of the coupon. For single coupons, the front or numbered side was facing downward during exposure. For the galvanic and crevice couples, the back or non-numbered side of the coupons were mated together.¹ In the galvanic couple, the front of the aluminum coupon was facing downward.

The 2014 surveillance coupons were visually different than the 2010 surveillance coupons. The 2014 coupons had a rust-like patina or particles on many of the coupons, especially on the upward facing surfaces as shown in Figure 4-1(A). This rust-like patina was noted on removal of the coupons from the basin. Previous coupons have not been observed with this feature as shown by the photographs in Appendix C for single configuration coupons and the 1100 galvanic couples. Many coupons removed in 2004 had discrete particles, which is attributed to settling particulate from the basin or spotting from corrosion of impurities or intermetallics anodic to the base metal.

¹ For galvanic couple 304 #044/Al 6063 #130, the front- or numbered-side of the 304L coupon was mated to the back side of the aluminum coupon.

The 2004 coupons were removed prior to the inadvertent discharge of the sand filter fines into the basin pool, which occurred in July 2004. All other coupons removed between 2006 and 2014 were exposed to this discharge to some degree. From the visual examination of coupons from 2005 to 2014, the surface features appear quite variable with heavy oxide formation and deposits on 2006 coupons to few deposit and minimal oxide on 2008 coupons. Since the surveillance coupons removed from 2006 to 2014 are made of the same heat of material, particles falling out from the basin water are most likely the cause for the rust-like patina or particles on the 2014 coupons. The incident would have occurred either after the 2010 removal or was localized to the area of the basin where the 2014 coupons were located.

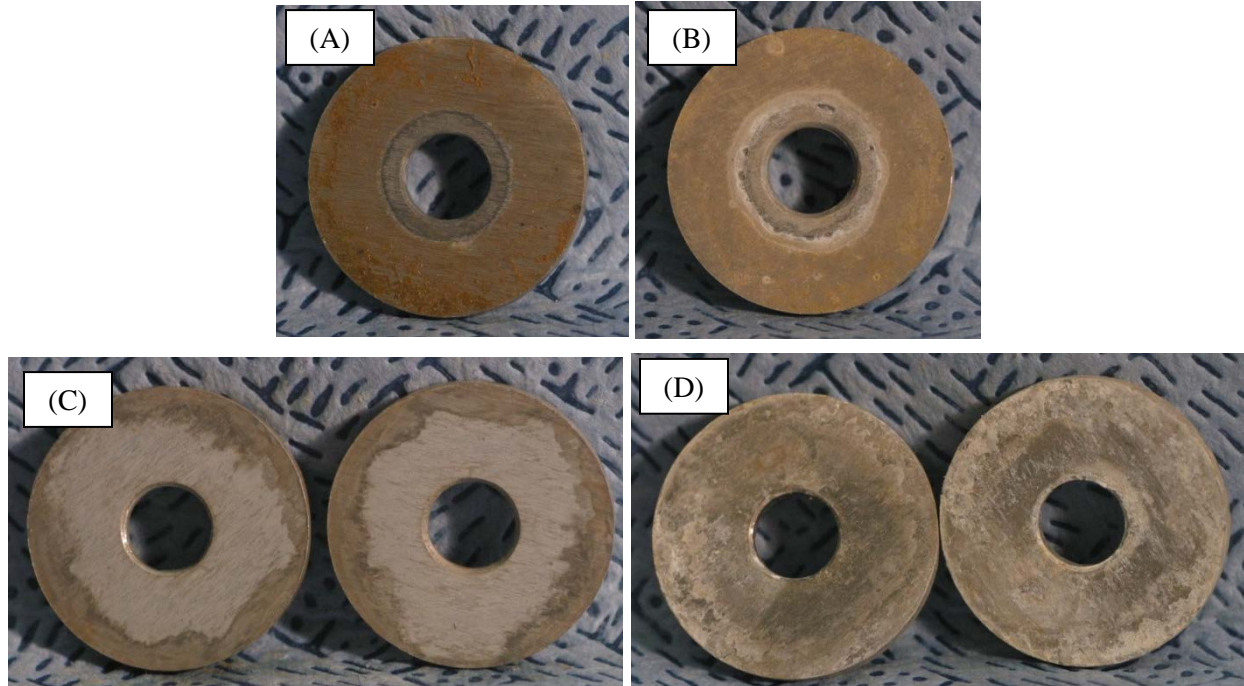


Figure 4-1. Photographs of 2014 L Basin surveillance coupons prior to cleaning: (A) single Al1100 coupon with rust-like patina; (B) single Al6061 coupon without rust patina; (C) mating surfaces from Al 6063 crevice couple; and (D) mating surfaces from Al1100 galvanic couple (304L on left, Al1100 on right).

Very broadly, the 2014 surveillance coupons developed a surface oxide, which led to a change in the surface color as shown in Figure 4-1(B). This oxide was non-uniform due to localized variations, including the formation of pits as well as the galvanic coupling and crevice effects. Within the crevices between the separation washer and the coupon, a buildup of white oxide formed near the washer edge. Mating surfaces of coupon couples showed a large buildup of oxide which had either a mottled appearance (galvanic couples, Figure 4-1(D)) or an irregular ring appearance (crevice couples, Figure 4-1(C)). The observed black oxide occurred mostly in a crevice. As can be seen from the data in Table 4-1, the corrosion morphology of the upward and downward facing surfaces differed visually for both single and couple configurations.

The 304L coupons in the galvanic couples showed minor discoloration with no detectable corrosion attack. Debris was obvious on the upward facing surfaces with rust-colored deposits or corrosion products as shown in Figure 4-2. Pitting corrosion was not apparent on the coupons. Surfaces that mated with an aluminum surface had a mottle appearance with a buildup of oxide from the aluminum coupons as shown in Figure 4-1(D). A thorough pit analysis of these 304L coupons was not performed since no apparent corrosion was observed.



Figure 4-2. Photographs of Al6061 galvanic couple with the 304L coupon surface facing upward and the Al6061 coupon surface facing downward

4.2 Surface Analysis

Surface analysis was performed on several of the 2014 surveillance coupons and included all alloys and coupon configurations. The analysis included XRD followed by SEM/EDS. The coupons were stored in basin water until the XRD analysis was performed. For this analysis, the coupons were not dried (i.e. residual water remained on the surface) to minimize changes in the oxide. After the XRD analysis, the coupons were no longer stored in water but exposed to air prior to SEM/EDS analysis. The SEM/EDS analysis focused on elemental analysis of the surface species. The upward facing surface of a coupon was evaluated. Polished disk coupons of each aluminum alloy were also examined to evaluate the inclusions and any impurities. These coupons were not from the 2014 surveillance JRG. The five 2014 coupons that were used for this work were 1100-033 (S), 1100-026 (G), 6061-091 (S), 6061-082 (C), and 6063-121 (S).

For all the coupons, gibbsite ($\gamma\text{-Al(OH)}_3$) and bayerite ($\alpha\text{-Al(OH)}_3$) were identified as the aluminum oxide phases present as shown in Figure 4-3 for 1100-026, which was in the galvanic couple (See Appendix D for a large image of this figure). For the basin pH range and low temperature of operation (i.e. $<77^\circ\text{C}$), a form of aluminum hydroxide (Al(OH)_3) known as nordstandite is predicted to form. Nordstandite can be considered a mixture of gibbsite and bayerite [9]. This result differs from the XRD results for 2006 and 2010 surveillance coupons where bayerite had a greater peak intensity than gibbsite, when it was present. [8, 10]. All oxide XRD peaks for these coupons generally are small compared to those resulting from the aluminum coupon. The 2006 and 2010 surveillance coupons were both dried ahead of performing the XRD which may have impacted the results.

The SEM/EDS analysis of the base metals showed there was a wide population of small intermetallic and impurity particles. Since the sizes were small ($10\text{ }\mu\text{m}$) as shown in Figure 4-4 and Figure 4-5, the chemical analysis data made isolation of specific compositions difficult because of the size of the EDS excitation volume. The elements identified are shown in Table 4-2 and are defined as primary and impurity ($<0.1\text{ wt\%}$). EDS spectra for the coupons exposed to the basin water had similar elements. The additional elements are identified in the table. Some of these additional elements identified on the surfaces of exposed coupons are also known as minor impurities in these alloys. These elements have been italicized in the table. Nearly every element identified on the surfaces of the exposed coupons could be from the alloy.

One species expected to be found was iron oxide because of the rust coloring on many of the coupons. Fe and O as dominant peaks were identified a few times. The SEM examination, however was not extensive and the presence of the rust-colored particulate was non-uniform. For the 6061 single coupon that was examined, Ag particulates were identified, although no reason can be given for why Ag was only found on one examined coupon or the source.

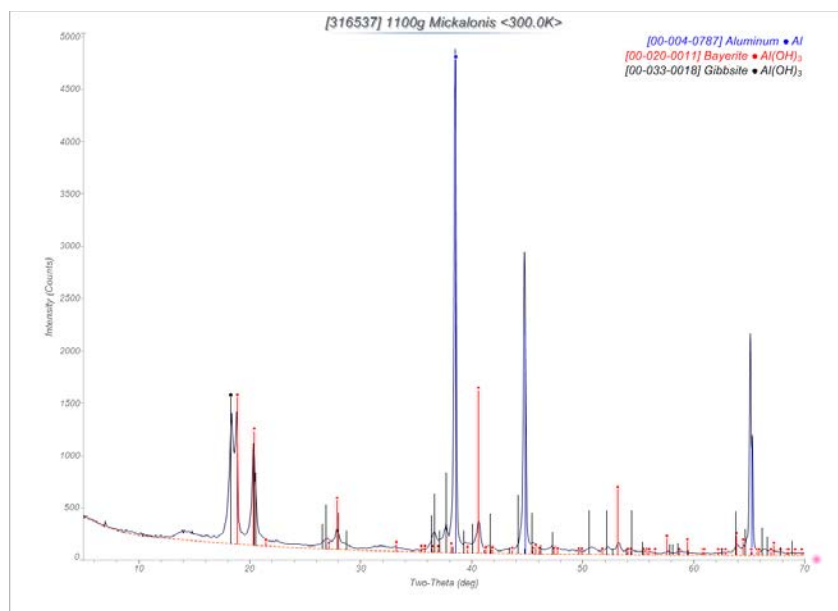


Figure 4-3. X-ray diffraction spectra for Al1100 galvanic coupon #026 downward facing coupon after a 15-year exposure in L Basin

Table 4-2. Elements Identified in Base Metal Alloys and Exposed Coupon Surfaces

Alloy	Base Composition		Exposed Coupon Surface*
	Primary	Impurity	
1100	Al, Si, Fe, Cu		<i>Mn</i> , Cr, Ca, Sb
6061	Al, Mg, Si, Fe, Cr, Cu		<i>Zn</i> , <i>Ti</i> , Ca, Ag
6063	Al, Si, Mg, Fe	Cu, Mn, Cr	<i>Zn</i> , <i>Ti</i> , Ca

*Italicized elements are a possible minor impurity for the alloy, but may have also deposited from the basin water

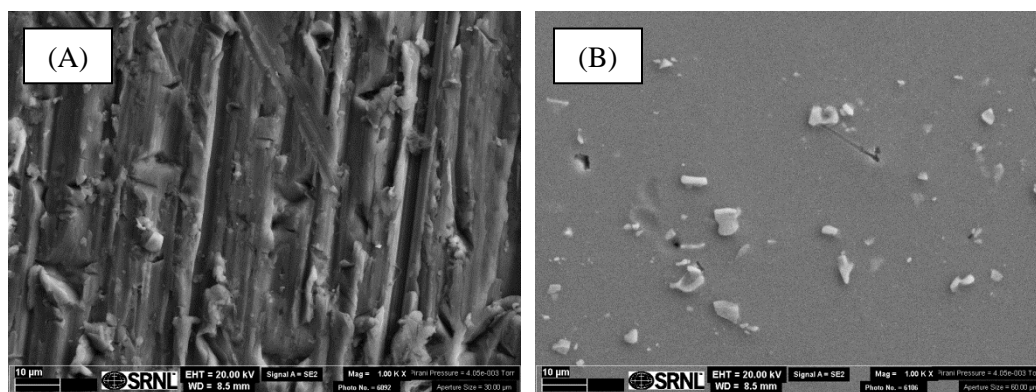


Figure 4-4. SEM micrographs showing intermetallic and impurity particles in base aluminum alloys: A) Al1100 (sample ground with 600-grit paper); and B) Al6061

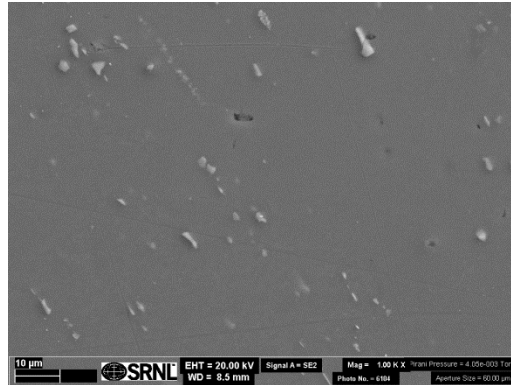


Figure 4-5. SEM micrographs showing intermetallic and impurity particles in base aluminum alloy Al6063

4.3 Impedance Spectroscopy

Impedance spectroscopy (EIS) is an electrochemical technique used to evaluate the time dependent processes of a system through small voltage or current perturbations. The system in this case is an oxide-covered aluminum surveillance coupon in an inert solution. In corrosion studies, EIS is generally employed to evaluate the corrosion processes occurring on the material in a solution of interest. In this case, EIS was used to non-destructively characterize the oxide that formed during exposure in the basin.

The impedance spectra for the single coupons of the three different alloys are shown in Figure 4-6 as a Nyquist plot, which shows the relationship between the real and imaginary impedance. The three spectra have similar shapes indicating a basic similarity in the oxide. The 6063 coupon does not reach the same imaginary component of the impedance as the 6061 and 1100 coupons so has a lower total impedance or resistance and a possible higher susceptibility to corrosion.

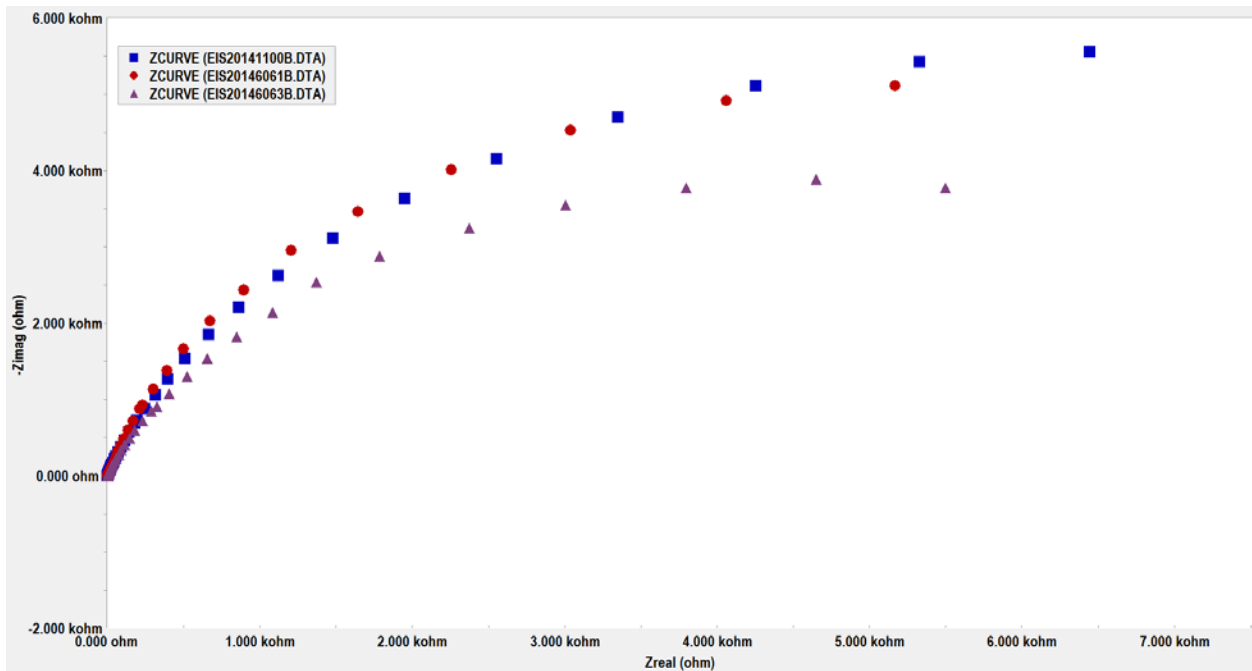


Figure 4-6. Nyquist plots for single coupons of each aluminum alloy, specifically 1100 #032, 6061 #093, and 6063 #123

Electrical circuit models are generally fitted to the impedance data to develop a better understanding of the processes and quantify these differences. Several standard models that are used to fit corrosion processes were tried with these data. In fitting a model, the most significant difference was seen in the resistance elements representing oxide and pore resistance with other elements representing a diffusional component and oxide capacitance being similar. The resistance values for 6063 were both smaller than those for 1100 and 6061, which were similar, and indicate the oxide film may not be as protective as those of 1100 and 6061.

4.4 Pitting Analysis

The pitting analysis followed the same approach used for previously removed coupons from L Basin and is based on ASTM G46 [6]. This analysis characterized the condition of pitting on the exposed coupons by identifying the deepest pit, calculating an average of the ten deepest measured pits, and determining a pit density. The pit depth measurement technique, however, differed this year with measurements made using a LCM; whereas, in previous years a measuring light microscope was used. A direct comparison was performed between these techniques using a coupon removed in 2010. Both this comparison and the complete analysis are discussed herein.

4.4.1 LCM-Light Comparison

The 2010 surveillance coupon chosen for the comparison of pit depth measurement techniques was the one used in 2010 for a complete pit count with the light microscope, a single coupon, 6061 #044 [8]. In this analysis, a pit depth minimum was set at 0.001 inch (1 mil), so anything less than that was not used. The 0.001 inch value was chosen since the focus was on the deepest pits. An advantage of the LCM is that if in the future an analysis of smaller pits is required, then the current LCM computer data file can be used. The standard pit parameters determined for measured pit depths by the two techniques are summarized in Table 4-3 along with the mean pit depth of the total number of measured pits on the coupon as well as those on an open surface not affected by crevices or the edge.

Table 4-3. Pit Parameters (inch) Determined Using the Light and the Laser Confocal Microscopes

Technique	Total #	Depth Range	Maximum Depth	10 Deepest Average	Mean \pm Std. Dev.	
					<i>All Data</i>	<i>Open Surface</i>
Light	49	0.0013-0.0039	0.0039	0.0017	0.0014 \pm 0.0006	0.0013 \pm 0.0004
Laser	45	0.0019-0.0025	0.0025	0.0021	0.0018 \pm 0.0007	0.0016 \pm 0.0003

In evaluating the data, pits that were located near the edge or in the area of the separation washer were not used in calculating the average of the 10 deepest pits, so these pits were not included in the total count given in the table. If all the data were included, the two data sets are statistically similar as shown by the mean and standard deviation given in Table 4-3. Each technique found a similar number of pits with depths greater than 0.001 inch, i.e. 49 and 45 for the light and laser microscopes, respectively. The pit ranges overlapped although the range does not give the whole picture since the light microscope depth measurements were generally smaller as indicated by the average of the 10 deepest pits as well as the means for all the measured pits and those on the open surfaces. If the maximum pit for the light microscope is not included, the range reduces to 0.0013-0.0016 inch with an average of 0.0014 inch; another indication that the light microscope measurements may be underestimating pit depth.

The pit depth distribution for each technique is given in Table 4-4 as another method of comparison (depth ranges are given in μm which is the measuring units of the LCM). The depth of the pits from the light microscope were again shown to be generally lower as shown by a greater distribution of pits in the 20-40 μm range than the 40-60 μm range, where the LCM was equally distributed between these two ranges. The reason for this difference may be associated with the uncertainty in identifying the bottom or top of the pit

in the light microscope technique. This uncertainty was further confirmed by different researchers measuring the same pit and comparing identified pit bottoms and tops.

Table 4-4. Measured Pit Depth Distribution from Light Microscope (LM) and Laser Confocal Microscope (LCM) Techniques

Depth (μm)	Frequency	
	LM	LCM
0-20	0	0
20-40	47	23
40-60	1	20
60-80	0	2
80-100	1	0

The 0.0039 inch pit for the light microscope (80-100 μm depth range) seems to be an outlier if not associated with an edge or washer or engraved number. One LCM pit measurement was excluded for being near a number, while no pit in the light microscope dataset indicates a pit associated with a number. By excluding this deep measurement from the light microscope dataset, the maximum pit, 10-pit average, and pit distribution are all less than those measurements made with the LCM, resulting in the two data sets being statistically different. This difference, however, does not invalidate previous light microscope measurements; especially the trend followed in the data over the last 15 years, which has shown no consistent large increase in pit depth. This comparison showed that the light microscope pit measurements appear to be less than those measured by the LCM, which removes human error in obtaining a focused spot for the measurements. Moving forward, a more representative value of the maximum pit will be identified and as shown below (Figure 4-8) the averages are only slightly impacted.

4.4.2 2014 Single Coupon Pit Analysis

The pit depths measured on the surveillance coupons removed in 2014 were similar for the three alloys as was their visual appearance. In Table 4-5, a summary of the pit depth data is provided including the average of the ten deepest pits, the depth range for those ten pits, the maximum pit depth for those pits not associated with the separation washer, edges or the engraved numbers, and the absolute deepest pit on the coupon.

As can be seen by these data, the differences between alloys are minimal and statistically there is no difference among the coupons, which can be seen graphically by the pit depth data presented in Figure 4-7 (units are in μm which is the measuring unit of the LCM). In previous coupon analysis, a comparison between the upward and downward faces have shown that no consistent face had deeper pits [8, 10, 14]. A significant difference was also not seen this year between the upward and downward facing surfaces. Again, similar to results from prior year coupons, the deeper pits were observed on the open face as opposed to the pits formed under the separation washer, i.e. a crevice pit [8, 14].

For the single coupons, the maximum pit depth measured on 2014 coupons was approximately three times higher than those measured on coupons removed in prior years, while the average depth was only slightly higher. The increase in maximum pit depth appears to be associated in part with the use of the LCM. From the discussion in the previous section on the comparison between LCM and light microscopy, pit depth measurements were found to have similar depth profiles. Deeper pits, however, were generally measured with the LCM although a three-time difference was not found. For this comparison, the one coupon was thoroughly examined by both techniques, which is generally not the case for most coupons that have been evaluated. Therefore, the possibility exists that on previous evaluations the deepest pit was not measured while the average depth gave a more accurate representation of the state of pitting. This point was also shown with the analysis performed with the 2010 surveillance coupons using only light microscopy [8].

Additionally, locating the bottom of a pit with the light microscope can be more challenging to obtain leading to shallower depth measurements.

Table 4-5. Pit-Depth (inch) Summary for 2014 Single Coupons

Alloy	Coupon #	Average Depth ^a	Depth Range	Open Maximum Depth ^b	Absolute Maximum Depth ^b	Pit Density (#/mm ²) ^c
6063	124	0.0050	0.0035-0.01	0.0100	0.0100	0.82/0.09
	123	0.0057	0.0035-0.0146	0.0146	0.0146	0.95/0.07
	122	0.0040	0.0031-0.0091	0.0091	0.0184	0.93/0.09
	121	0.0034	0.0029-0.0067	0.0067	0.0067	1.08/0.07
6061	94	0.0032	0.0024-0.0046	0.0046	0.0374	0.12/0.03
	93	0.0037	0.0024-0.0077	0.0077	0.0083	0.16/0.05
	92	0.0045	0.0025-0.0172	0.0172	0.0172	0.16/0.05
	91	0.0045	0.0029-0.0081	0.0081	0.0081	0.19/0.03
1100	33	0.0037	0.0027-0.0075	0.0075	0.0075	0.11/0.05
	32	0.0055	0.0043-0.0099	0.0099	0.0099	0.47/0.09
	31	0.0056	0.0033-0.0087	0.0087	0.0104	0.37/0.12
	20	0.0030	0.0026-0.0043	0.0043	0.0132	0.32/0.11

^aAverage of ten deepest pits on the open surfaces of each coupon

^bMaximum depth is for open surfaces; absolute maximum includes pits under washers, near edges or numbers

^c $\Sigma 4 \times 6$ LCM frame area pit (>1 mil) count/Total number of pits on front and back

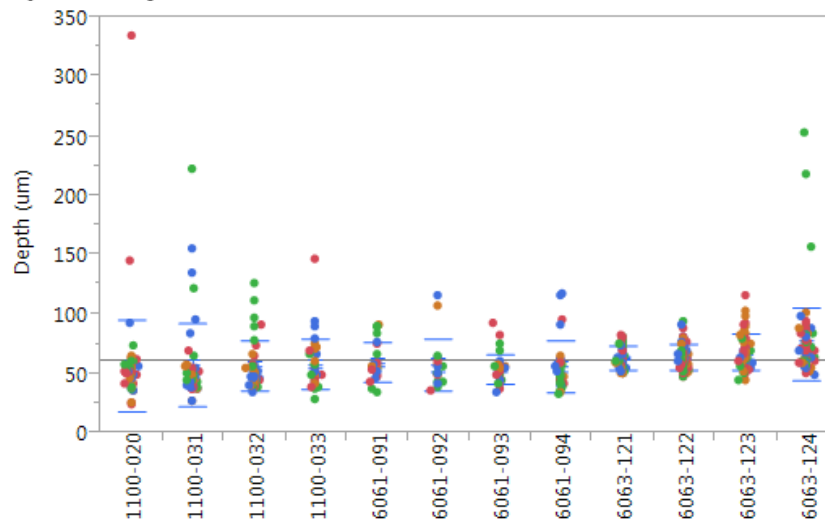


Figure 4-7. Plot of mean pit depth (>25.4 μm (1 mil)) and standard deviation for each 2014 surveillance coupon (the solid line indicates the overall average mean for this data set; color indicates the different quarter the pit was located)

The pit depths measured this year are in general the highest measured thus far for the coupons inserted into the basin in 1999. The trends of pit depth (absolute maximum and the average of the 10 deepest) from 2005 to 2014 are shown in Figure 4-8. These data do not differentiate between the back and front of the coupons, i.e. upward or downward orientation, which have shown similar depths. As can be seen by the data in Figure 4-8, the maximum pit depth measured in 2014 is significantly larger than previous

years. The 2014 maximum pit depths range from 10 to 16 mils for the three alloys. Previous years maxima were in a tight range of 3-5 mils.

The large increase in maximum pit depth was unexpected. Besides the difference in measuring technique, another difference found between the coupons from 2014 and those removed previously is the variation in surface deposits as shown in Appendix C with a pictorial comparison for the three alloys of representative coupons from each removal between 2005 and 2014. Coupons removed in 2005 and 2006 had a layer of sand particulate resulting from the startup of a new sand filter in July 2004 [10]. Coupons from 2008 and 2010 had a minimal amount of debris [8, 14]. For 2014 coupons there is the presence of the rust-colored debris with EDS identified iron particulate. Iron is known to be cathodic to aluminum so aluminum would corrode in preference to the iron. The iron in fact may act as a pit initiator and accelerate pit growth by depolarizing the cathodic reaction of oxygen reduction [15]. The deepest pit however was not always associated with a thick layer of particulate, i.e. A1100 #32 (see Appendix B). The timeframe that these particulates deposited on the aluminum surface is unknown.

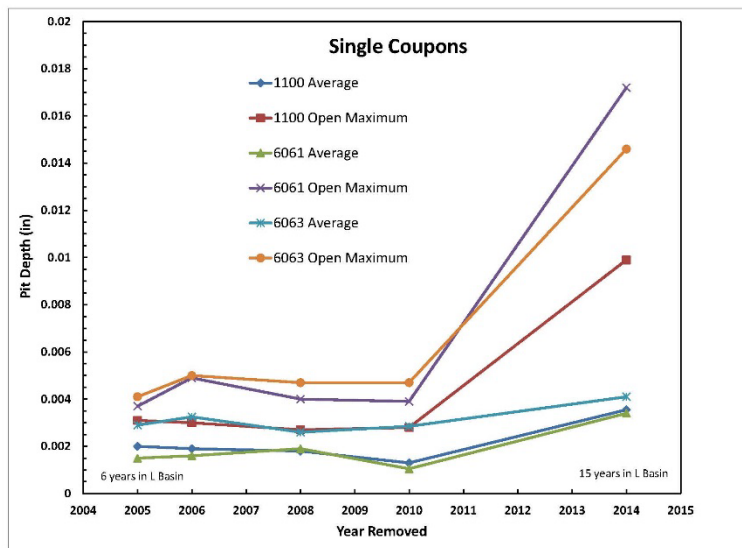


Figure 4-8. Trend plot of the maximum and the 10-deepest average pit depths for single surveillance coupon from 2005 to 2014

Another contributing factor may be the amount of residual oxide on the surface during pit measurement. During the 2014 analysis, every effort was made to remove the oxide. Examining notes from analyses performed for coupon removed previously, an indication is given that all the oxide was not removed on some coupons, which may have skewed the results due to failing to measure the pits below that oxide.

Another difference in the 2014 data is the variability in the maximum pit depth. In Table 4-6, the range of values is given for the maximum pit depths as a function of removal year. Two maximum pit depths are shown; the open depth is for pits not associated with crevices or edges and the absolute depth is the absolute deepest pit on a coupon. From these data, the range of maximum depths for 2014 coupons generally has the largest difference between the smallest and largest depth as well as the highest percentage difference between smallest and largest depths. The 6063 coupons have the greatest similarity over all the years.

Table 4-6. Range of Maximum Pit Depths for Surveillance Coupons Removed from L Basin Between 2005 and 2014

Year Removed	1100 Range of Maximum Pit Depth (mils)		6061 Range of Maximum Pit Depth (mils)		6063 Range of Maximum Pit Depth (mils)	
	Open	Absolute	Open	Absolute	Open	Absolute
2014	4.2-9.9	7.5-13.2	4.6-17.2	8.1-20.	6.7-14.6	6.7-18.4
2010	1.9	2.3-5.6	1.2-1.6	1.6-2.6	2.3-4.7	3.5-4.7
2008	1.9-2.7	2.-6.0	3.1-4.0	3.1-4.0	3.6-4.7	3.6-4.7
2006	1.8-2.5	2.5-3.0	3.1-4.2	3.1-4.9	4.3-5.0	4.3-5.0
2005	2.5-2.8	2.5-3.1	1.8-3.7	ND	2.-4.1	3.6-4.1

The surveillance coupons have been exposed throughout the basin as shown by the data in Table 4-7. In the basin map shown in Figure 2-1, the location of the previous removals are shown by green-colored boxes with the removal date. Chemical analysis of water samples taken from the basin at different locations and heights has shown that the water chemistry is independent of location [16]. Location, however, does seem to impact particulate deposition. Evaluating location with the type of surface layer does not provide additional insight. Stagnant areas probably exist which may have resulted in some locations having greater deposition, especially from the sand filter in 2004 when the whole basin was cloudy. The presence of iron on the 2014 coupons may indicate localized activities in the basin. A review of coupons removed in 2004 (which were immersed in 1996) revealed discreet large rust-colored debris. The location of the 2004 coupons inside the basin is unknown.

Table 4-7. Corrosion Surveillance Coupon Exposure Location in L Basin

Year Removed	Years in Basin	Basin Location*	Surface Layer
2005	5.9	VTs - center	Thin, sand
2006	7	HTS - west	Heavy, sand
2008	9.1	HTS - center	None
2010	11	VTs	None
2014	15.4	HTS - east	Non-uniform, iron

*HTS – horizontal tube storage, VTs – vertical tube storage,

The average of the ten deepest for 2014 shown in Table 4-5 is the average of the ten deepest pits found on either the back or front of the coupon. In analyses from previous years, the ten deepest pit averages were the mean of the ten deepest pit averages from both sides, back and front. The 2014 approach is an improved measure of degradation and made easier by improvement to the pitting analysis. The previous method produces a slightly smaller average pit depth, although still representative of the exposed coupons. As can be seen by the trend line of the average pit depth, the data falls within a tight band and has only a slight uptick resulting from the larger 2014 measurements.

The pit density measured for the 2014 coupons were generally less than 1 pit/mm² for pit depths greater than 1 mil. These data are shown in Table 4-5. In previous analysis, the pit density values were substantially higher. The pit density values ranged between 20 and 100 pits/mm² for the years 2005-2008 [14]. This difference falls in part to the approach taken. In 2014, eight 4×6 LCM frame area (~27.4 mm²) values were measured for each coupon, one from the four quarters of each surface (front and back). Previously, coupons were examined with locations chosen based on a visual assessment of a high density of pits and the pit count performed while examining the coupon at 200X (~0.5809 mm²). Pits with depths less than 1 mil may have been counted. If pits between 0.5 and 1 are included in the 2014 for the 4×6 area, the pits density value increase by a factor of 2 to 10, but clearly still below the pit density values measured in previous years.

In Table 4-5, two density values are given – number of pits in 4×6 area/total number of pits on both sides of coupons. In both cases these are for pit depths greater than 1 mil. As can be seen by these data, the 4×6 area overestimated the coupon pit density based on the total number of pits counted. Since the pit density analyses performed in previous years used even a smaller area perhaps a large overestimation occurred. In future analysis with the LCM, the 4×6 area may offer a convenient and less time-consuming method for the pit density measurements, realizing the value is conservative and that the real density may be an order of magnitude less.

As seen by the various measures for pit characterization, ten deepest average, maximum pit depth, and pit density, the three alloys showed very similar values. No alloy appears to be significantly less corrosion resistant than the other, although the EIS results indicate that 6063 may be slightly less resistant than 1100 or 6061.

4.4.3 2014 Crevice Coupon Pit Analysis

The 2014 crevice coupons generally continued the trend of slightly increasing pit depths with time observed with previous crevice couples as shown by the data in Figure 4-9 for the crevice couples removed between 2005 and 2014. As for the single coupons, the greater depths are observed for the 2006 and 2014 coupons.

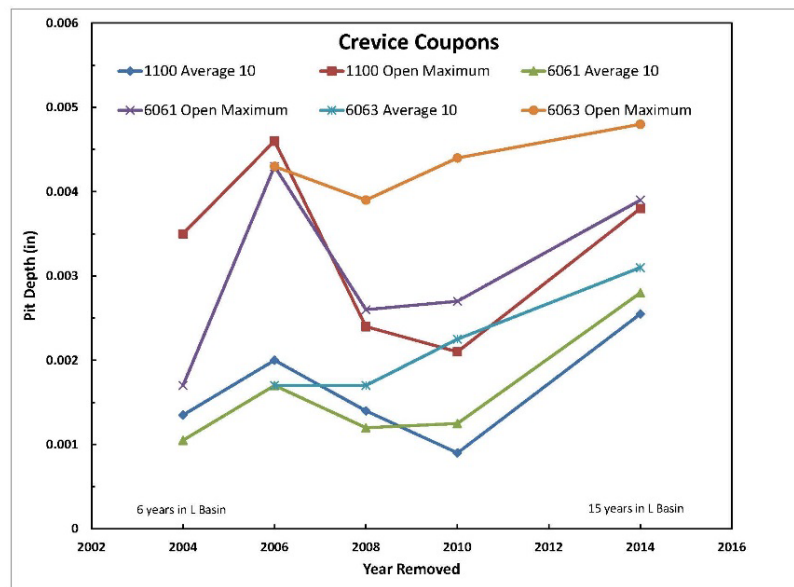


Figure 4-9. Trend plot of the maximum and 10-deepest average pit depths for crevice surveillance coupon from 2005 to 2014

A summary of the average pit depth, maximum depths and pit density is shown in Table 4-8 for the 2014 crevice couples. As can be seen by the 2014 data, the two coupons in a couple performed similarly with the largest differences in the maximum pit depths. The average and density were close in value. In the crevice couple, the 1100 and 6061 alloys behaved similarly while 6063 had greater pit maximums and pit density, especially #127/#128 with values greater than the 1 pit/mm² and an absolute maximum depth of 0.0131 inch. Visually, this couple appeared similar to the others (See Appendix B).

Unlike the single coupons, a difference in the average or maximum depth was seen between the front and back side. The back sides of the two coupons in the couple were mated together to form the crevice. The back side generally had the largest average and maximum pit depth indicating a more aggressive condition

within the crevice, as would be expected. The pit density was also significantly less. The pit density given in Table 4-8 is only the front side average density. On the back side, there were insufficient pits to calculate a pit density in the 4×6 area, which indicates the pit density within the crevice is quite small. Similar to the single coupons if the total area of a side and total pit count is used to calculate the density, then the pit density will be much smaller.

Table 4-8. Pit-Depth (inch) and Density Summary for 2014 Crevice Coupons

Alloy	Couple/ Coupon	Average Depth*			Maximum Depth		Pit Density (#/mm ²) ^Σ
		Total	Front	Back	Front/Back*	Absolute	
6063	1/125	0.0042	0.0042	0.0019	0.0046/0.0027	0.0145**	0.6
	1/126	0.0032	0.0031	0.0023	0.0042/0.0038	0.0042**	0.52
	2/127	0.0048	0.0033	0.0042	0.0038/0.0131	0.0131	1.79
	2/128	0.0037	0.0037	0.0024	0.0048/0.0029	0.0048	1.14
6061	3/81	0.0037	0.0020	0.0037	0.0023/0.0043	0.0043	0.09
	3/82	0.0035	0.0024	0.0035	0.0032/0.0057	0.0057	0.11
	4/97	0.0026	0.0021	0.0026	0.0024/0.0033	0.0033	0.3
	4/98	0.0035	0.0027	0.0033	0.0039/0.0039	0.0039	0.38
1100	5/27	0.0040	0.0026	0.0039	0.0038/0.0062	0.0062	0.07
	5/28	0.0032	0.0020	0.0035	0.0024/0.0066	0.0066	0.08
	6/29	0.0026	0.0025	0.0017	0.0032/0.0028	0.0032	0.12
	6/30	0.0023	0.0021	0.0022	0.0024/0.0025	0.0033**	0.13

*Numbered side(front) for open surface/Non-numbered side (back and mating surface of couple)

**Associated with front washer

ΣThe density is from the 4×6 area

4.4.4 2014 Galvanic Aluminum Coupon Pit Analysis

The 2014 galvanic coupons had pit depths very similar to those measured previously as shown by the trend plot of the average and maximum pit depths in Figure 4-10 for the galvanic couples removed between 2005 and 2014. A summary of the average pit depths, maximum depths and pit density is shown in Table 4-9 for the 2014 galvanic couples. As can be seen by a comparison of the data in the table, the alloys performed similarly.

Table 4-9. Pit-Depth (inch) and Density Summary for 2014 Galvanic Coupons

Alloy	Coupon #	Average Depth*			Maximum Depth		Pit Density (#/mm ²) ^Σ
		Total	Front	Back	Open*	Absolute	
6063	129	0.0193	0.0124	0.0136	0.0085/0.0161	0.0683 ^β	0.22
	130	0.0170	0.0107	0.0150	0.0233/0.0189	0.0233 ^β	0.35
6061	95	0.0172	0.0106	0.0148	0.0255/0.0209	0.0255 ^β	0.11
	96	0.0137	0.0043	0.0133	0.0141/0.0167	0.0172	0.09
1100	25	0.0112	0.0094	0.0107	0.0121/0.0148	0.0333 ^β	0.44
	26	0.0093	0.0081	0.0087	0.0124/0.0107	0.0180 ^β	0.24

*Numbered side(front)/Non-numbered side (back and mating surface of couple)

ΣFront side average pit density only

βMaximum pit depth on front side

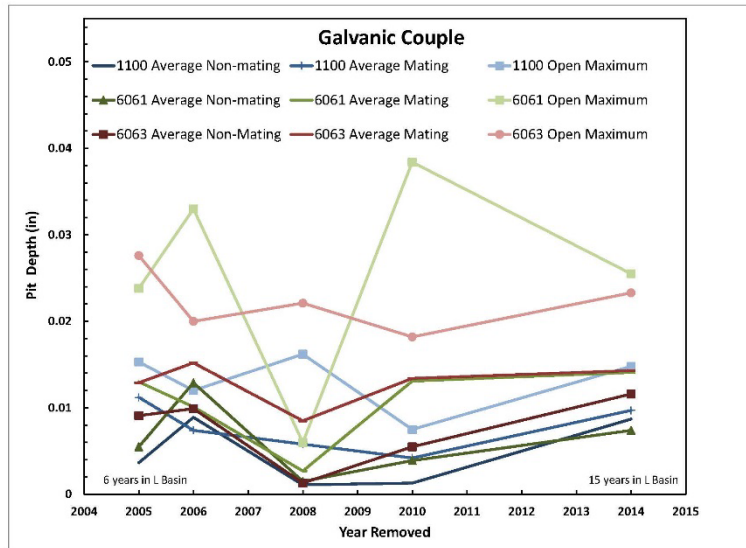


Figure 4-10. Trend plot of the maximum and average pit depth for galvanic surveillance coupon from 2004 to 2014

By comparison of the data in Table 4-9 with that in Table 4-5 and Table 4-8, the pit depths can be seen to be greater along with a higher pit density for the galvanic couples than the other coupon configurations. These greater depths are attributed to the galvanic interaction with the stainless steel coupon and the resulting increased cathodic reaction rate. The back or mating side of the galvanic coupons, similar to the crevice coupons, has a higher average pit depth, which is also similar to coupons removed in previous years (see Figure 4-10). Many of the absolute maxima on the 2014 galvanic coupons were associated with the edge, number or separation washer on the non-mating side.

The 2014 maximum pit depth, however, is greater on the front or non-mating side. This result is similar to the coupons removed in 2006, but runs counter to those coupons removed in other years. The reason for this difference is not clear since the front side of the aluminum coupon in the galvanic couple is facing downward and would not be impacted by debris on the surface. Although the front side could be impacted by the galvanic interaction, difference in oxide thickness and the resistant to corrosion may differ among the various coupons. Differences in the tightness of the crevice could impact the oxide growth within the crevice. Evaluation of coupons prior to cleaning, however, showed no visual evidence as shown by the pictures of representative galvanic couples in Appendix C with 1100 for the years 2005-2014.

5.0 Discussion

During the analysis of the 2014 corrosion surveillance coupons, removed from L Basin after 15 years, the use of a LCM was initiated to provide an improved measure for pit characterization. The comparison of this technique with the manual light microscope measurements used previously showed that the population of measured pits were different. Also, depending on the treatment of the data, this difference could be statistically different, especially for single coupons. The difference in pit depths between the two techniques is believed to be associated with the greater challenge of identifying the bottom of a pit using the light microscope, as well as an improved capability of determining oxide within the pit using the LCM. Even with these differences, the average pit depth of the ten deepest pits have shown to be similar and provide a continuity in aluminum corrosion measurement. Using the LCM provides a better measure of the maximum pit depth and subsequent potential for penetrating the cladding.

The purpose of the L Basin corrosion surveillance program is to provide a measure of the corrosiveness of the basin water chemistry to the stored aluminum-clad spent nuclear fuel. This corrosion is monitored by trending pit depth parameters for the three coupon configurations, which were shown in Figures 4-7 to 4-9. These data continue to demonstrate that pitting is a stochastic process and varies depending on all conditions impacting corrosion. As has been shown consistently for the current set of coupons installed in L Basin in 1999, the well-maintained chemistry of the basin water is not the primary variable impacting aluminum corrosion. Although chloride even at <1 ppm level is the primary aggressive species, the continuous low levels over the last fifteen years does not explain the pit depth variability.

If the trends observed for the three coupon configurations are evaluated collectively (Figures 4-7 to 4-9), a consistent variation is seen that appears to be primarily impacted by the deposition of debris on the surface. As shown by the data presented in Table 4-7 and the visual appearance of representative coupons shown pictorially in Appendix C, a debris layer as found on coupons removed in 2005, 2006 and 2014 corresponds to greater pit depths. These years had the higher average and maximum pit depths and gave the trend curves a saddle appearance. Currently, the deposition of this debris cannot be predicted by location of the coupons in L Basin as shown by the data in Table 4-7. A review of L Basin operation is recommended to assess whether activities in the basin may be making conditions for the exposed coupons different at their various exposure locations.

The single coupons were most significantly impacted by the deposition of the iron particulate observed on the 2014 coupons as determined by the difference in pit depth compared with previous years. The larger increases for the single coupons may be associated with both the accelerating impact of iron on aluminum corrosion and the lack of influence by a crevice as for the crevice couple. In the galvanic couple, the aluminum coupon was downward facing so the iron particulate would not have as big an effect on the aluminum corrosion.

As observed on previous coupons, the pitting associated with the galvanic couples was generally greater due to the electrochemical driving force associated with the 304L coupons, similar to interaction of the iron particulate with the aluminum surface. These higher rates can be seen by comparing the pit depths in Table 4-5, Table 4-8, and Table 4-9 for the single, crevice couple, and galvanic couple, respectively. Since the galvanic couples also have a crevice, the pitting within the crevice was also where the greatest corrosion was observed for this set of coupons. Besides the driving force from the 304L coupling, oxygen depletion and solution acidification, which can occur within a crevice, would accelerate the pitting.

The measured pit depths for the crevice couples were similar to those for the single coupon configuration including the pit depths within the crevice. The similarity in measurements may be associated with the tightness of the crevice or the development of oxide on the two surfaces. A looser crevice would minimize the depletion of oxygen and the solution acidification. A thickening oxide layer would tend to increase the resistance to diffusional changes through the solution or to increase the resistance to corrosion.

Work has been initiated to statistically evaluate the different data sets of coupons removed from L Basin between 2005-2014. Since these coupons are all from the same lot of material, a material difference is removed as a major factor for observed difference in pit depths. With this stated, the corrosion is primarily impacted by the actual surface characteristics of any coupon, which can have a varying intermetallic and impurity density. Using a statistical evaluation will aid in determining the significance of the observed differences.

6.0 Conclusions

The results of the 2014 surveillance coupon analysis continue to demonstrate that the well-controlled basin water chemistry has been managed to keep aluminum corrosion at low levels for the aluminum cladding on

the spent nuclear fuel and the basin storage racks. The use of the LCM to make the pit measurements provides a better method at identifying the maximum deepest pit, which provides the best measure for when the aluminum cladding would be compromised, as well as more representative values of average pit depths and pit density. The maximum pit depths on open surfaces for the three alloys, 1100, 6061 and 6063 were 0.01, 0.017, and 0.015 mils, respectively.

The 2014 results continue to demonstrate that galvanic interactions are aggressive accelerators of aluminum corrosion whether the interaction results from coupling with stainless steel components or the deposition of rust on aluminum surfaces. The absolute pit depth maxima associated with galvanic interactions were 0.015, 0.026, and 0.023 mils, for 1100, 6061 and 6063, respectively. Although intentional galvanic couples between 304L and aluminum components are no longer a concern in L Basin, this type of corrosion acceleration, however, may still be a concern due to deposition of iron oxides on to aluminum components as was observed on the 2014 surveillance coupons.

The trend in maximum and average pit depths for coupons removed between 2005 and 2014 (immersed in 1999) showed that the greater depths were associated with the presence of a surface deposit. From a review of the exposure location in the basin for each set of coupons, a cause for the observed variation in deposition of particulate on the coupon surface could be determined. A review of L Basin operation is recommended to assess whether activities in the basin may be making conditions for the exposed coupons different at their various exposure locations.

The water quality throughout the 2005-2014 period has been good with few chemistry excursions and within the parameter limits established for basin operation that are consistent with international guidelines for aluminum fuel storage. The incidence of pitting is not expected to be mitigated by more stringent control of the water quality. Changes to the current removal schedule of the L Basin Corrosion Surveillance Program are not recommended at this time. Further development of the measurement protocol using statistical analysis will be undertaken with a goal to reduce the time to perform the analysis and to reduce storage capacity of the data.

7.0 References

1. 2009 IAEA Nuclear Energy Series No. NP-T-5.2, "Good Practices for Water Quality Management in Research Reactors and Spent Fuel Storage Facilities," International Atomic Energy Agency, Division of Nuclear Fuel Cycle and Waste Technology, Research Reactor Section, 2011
2. International Atomic Energy Agency, "Corrosion of Research Reactor Aluminum Clad Spent Fuel in Water," IAEA-TRS-418, IAEA, Vienna, 2003
3. ASTM International G1 – 03 (Reapproved 2011), "Standard Practice for Preparing, Cleaning, and Evaluating Corrosion Test Specimens," ASTM International, West Conshohochen, PA, 2013
4. ASTM International G4 – 01 (Reapproved 2008), "Standard Guide for Conducting Corrosion Tests in Field Applications," ASTM International, West Conshohochen, PA, 2013
5. ASTM International G46 – 94 (Reapproved 2013), "Standard Guide for Examination and Evaluation of Pitting Corrosion," ASTM International, West Conshohochen, PA, 2013
6. J. I. Mickalonis, "L Basin Corrosion Surveillance Program Plan," SRNL-TR-2009-00140, Revision 3, September 2014
7. Email communication, R. Deible to J. Mickalonis October 20, 2014
8. J. I. Mickalonis et al, "L Basin Corrosion Surveillance Program Plan – Evaluation of 2010 Surveillance Coupons," SRNL-TR-2014-00004, June 2015

9. E. Shaber and G. Hofman, "Corrosion Minimization for Research Reactor Fuel," INL/EXT-05-00256, Revision 0, June 2005
10. P. R. Vormelker and C. N. Foreman, "FY2005 and FY2006 Corrosion Surveillance Results for L Basin," SRNL-TR-2007-00342, September 2007
11. SRNL Laboratory Notebook, SRNL-NB-2006-00129, "2006 L Basin Coupon Corrosion Surveillance," active dates October 2, 2006 to September 15, 2009
12. P. R. Vormelker, A. J. Duncan, and D. W. Vinson, "FY 2002/FY2003 Corrosion Surveillance Results for the SRS Basins," WSRC-TR-2003-00548, December 2003
13. P. R. Vormelker, A. J. Duncan, and T. R. Murphy, "FY2004 Corrosion Surveillance Results for L Basin," WSRC-TR-2005-00067, September 2005
14. P. R. Vormelker and C. N. Foreman, "FY2008 Corrosion Surveillance Results for L Basin," SRNL-TR-2009-00256, December 2009
15. J. E. Hatch (ed.), Aluminum: Properties and Physical Metallurgy, American Society for Metals, Metals Park OH, 1984
16. R. W. Deible, "Spent Fuel Storage Basin Water Chemistry Control Program," WSRC-TR-97-0239, Rev. 5, June 2010

Appendix A 2014 Surveillance Coupon Numbers and Configurations
2014 Surveillance Coupon Position, Numbers, Type, and Analyses.

Position*	Type**	Alloy	Number	Numbered Side		Analyses Performed
				Up	Down	
1	S	1100	033		X	XRD/SEM
2	S	1100	032		X	EIS/Pitting
3	S	1100	031		X	Pitting
4	S	1100	020		X	Pitting
5	S	6061	091		X	XRD/SEM
6	S	6061	092		X	Pitting
7	S	6061	093		X	EIS/Pitting
8	S	6061	094		X	Pitting
9	S	6063	121		X	XRD/SEM
10	S	6063	122		X	Pitting
11	S	6063	123		X	EIS/Pitting
12	S	6063	124		X	Pitting
13	G	304	011	X		Pitting
	G	1100	026		X	XRD/SEM
14	G	304	012	X		EIS/Pitting
	G	1100	025		X	Pitting
15	G	304	041	X		Pitting
	G	6061	096		X	EIS/Pitting
16	G	304	042	X		Pitting
	G	6061	095		X	Pitting
17	G	304	043	X		Pitting
	G	6063	129		X	Pitting
18	G	304	044		X	Pitting
	G	6063	130		X	EIS/Pitting

Position*	Type**	Alloy	Number	Numbered Side		Analyses Performed
				Up	Down	
19	C	1100	027	X		Pitting
	C	1100	028		X	Pitting
20	C	1100	029	X		Pitting
	C	1100	030		X	Pitting
21	C	6061	082	X		XRD/SEM
	C	6061	081		X	Pitting
22	C	6061	098	X		Pitting
	C	6061	097		X	Pitting
23	C	6063	128	X		Pitting
	C	6063	127		X	Pitting
24	C	6063	126	X		Pitting
	C	6063	125		X	Pitting

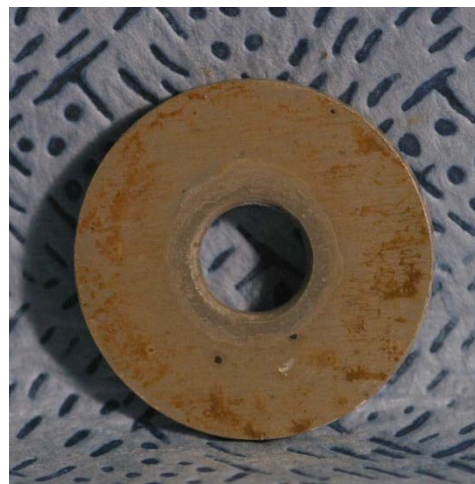
Appendix B 2014 Surveillance Coupon Photographs – Before and After Cleaning

Al 1100 #020

As-received from L Baisn



Downward



Upward

After cleaning in nitric acid solution



Downward



Upward

Al 1100 #031

As-received from L Baisn



Downward



Upward

After cleaning in nitric acid solution



Downward



Upward

Al 1100 #032

As-received from L Baisn



Downward



Upward

After cleaning in nitric acid solution



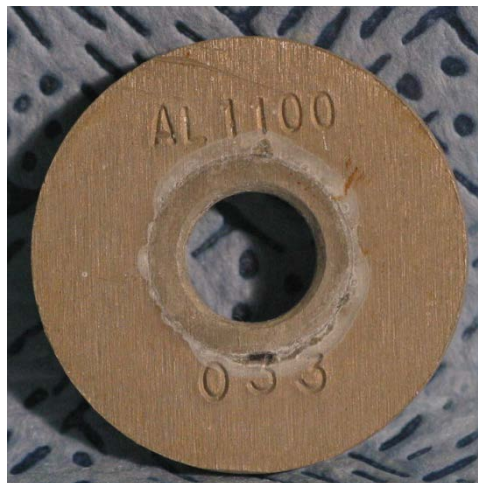
Downward



Upward

Al 1100 #033

As-received from L Baisn



Downward

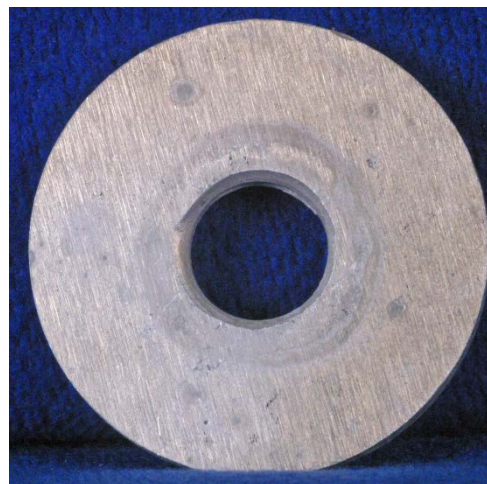


Upward

After cleaning in nitric acid solution



Downward



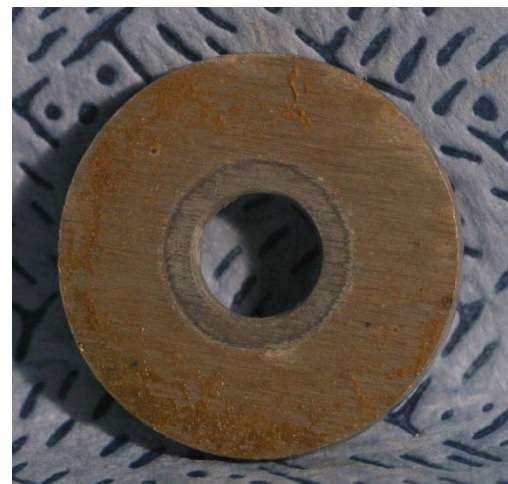
Upward

Al 6061 #091

As-received from L Baisn



Downward



Upward

After cleaning in nitric acid solution



Downward



Upward

Al 6061 #092

As-received from L Baisn



Downward

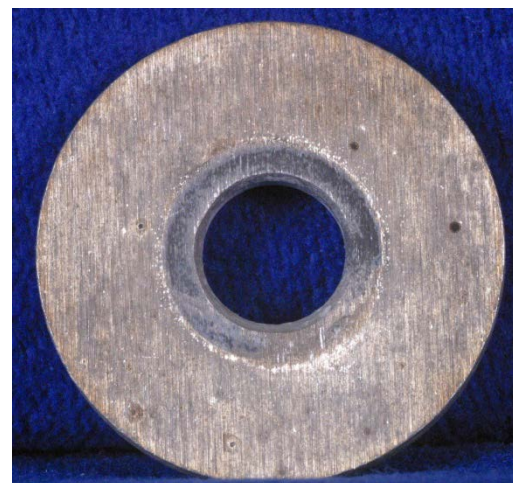


Upward

After cleaning in nitric acid solution



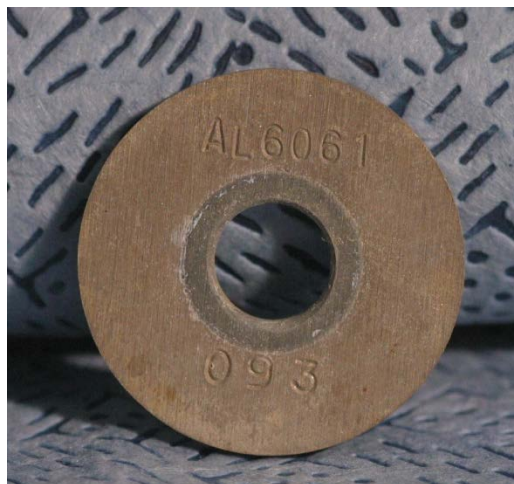
Downward



Upward

Al 6061 #093

As-received from L Baisn



Downward



Upward

After cleaning in nitric acid solution



Downward



Upward

Al 6061 #094

As-received from L Baisn



Downward



Upward

After cleaning in nitric acid solution



Downward



Upward

Al 6063 #121

As-received from L Baisn

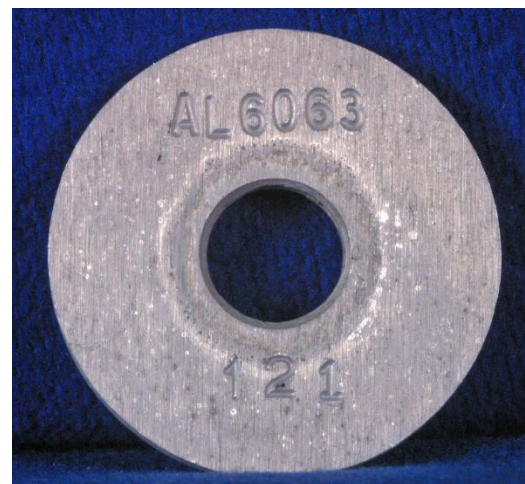


Downward



Upward

After cleaning in nitric acid solution



Downward



Upward

Al 6063 #122

As-received from L Baisn



Downward



Upward

After cleaning in nitric acid solution



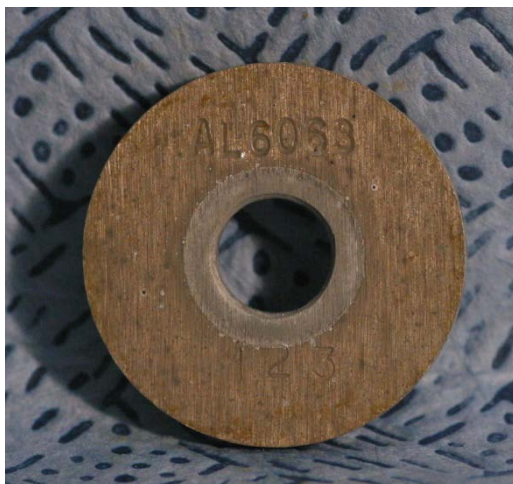
Downward



Upward

Al 6063 #123

As-received from L Baisn



Downward



Upward

After cleaning in nitric acid solution



Downward



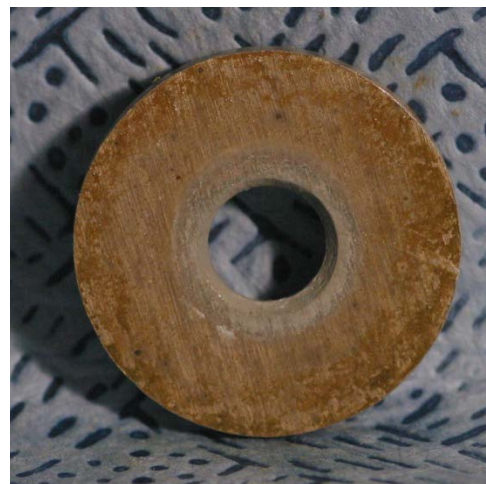
Upward

Al 6063 #124

As-received from L Baisn



Downward



Upward

After cleaning in nitric acid solution



Downward



Upward

304 #011/Al 1100 #026

As-received from L Baisn



Upward/Downward



Coupled Surfaces-304/1100

After cleaning in nitric acid solution



304 #011



1100 #026

304 #012/Al 1100 #025

As-received from L Baisn



Upward/Downward



Coupled Surfaces-304/1100

After cleaning in nitric acid solution



304 #012



1100 #025



304 #041/Al 6061 #096

As-received from L Baisn



Upward/Downward



Coupled Surfaces-304/6061

After cleaning in nitric acid solution



304 #041



6061 #096

304 #042/Al 6061 #095

As-received from L Baisn

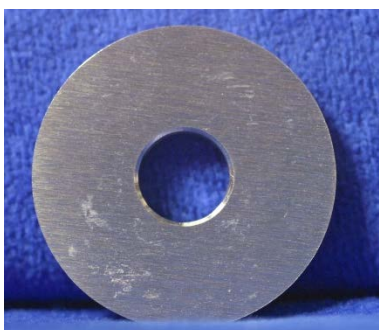


Upward/Downward



Coupled Surfaces-304/6061

After cleaning in nitric acid solution



304 #042



6061 #095

304 #043/Al 6063 #129

As-received from L Baisn



Upward/Downward



Coupled Surfaces-304/6063

After cleaning in nitric acid solution



304 #043



6063 #129

304 #044/Al 6063 #130

As-received from L Baisn



Upward/Downward

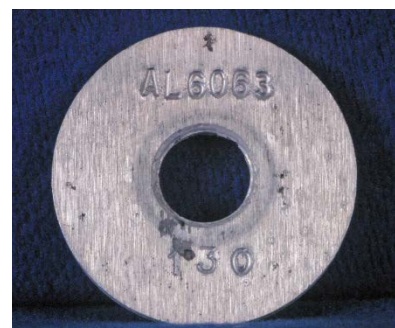


Coupled Surfaces-304/6063

After cleaning in nitric acid solution



304 #044



6063 #130

Al 1100 #027/Al 1100 #028

As-received from L Baisn



Upward/Downward

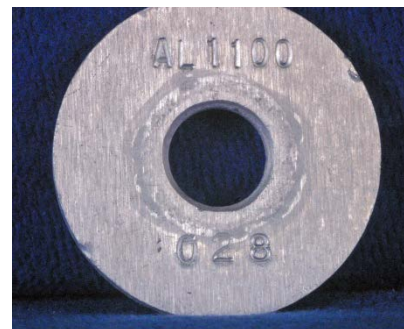


Creviced Surfaces

After cleaning in nitric acid solution



Al 1100 #027



Al 1100 #028

Al 1100 #029/Al 1100 #030

As-received from L Baisn



Upward/Downward



Creviced Surfaces

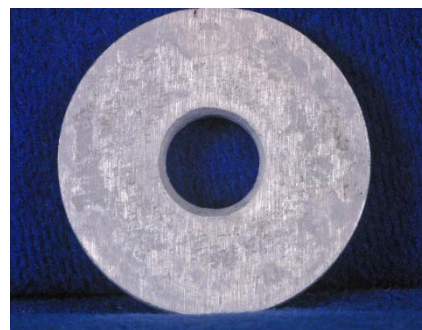
After cleaning in nitric acid solution



Al 1100 #029



Al 1100 #030



Al 6061 #082/Al 6061 #081

As-received from L Baisn

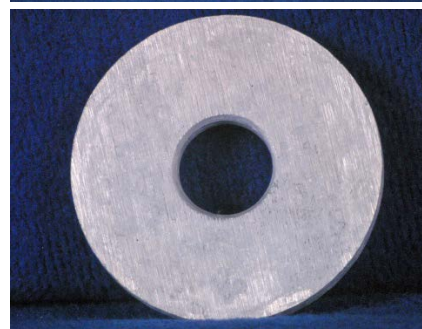


Upward/Downward



Creviced Surfaces

After cleaning in nitric acid solution



Al 6061 #082



Al 6061 #081

Al 6061 #098/Al 6061 #097

As-received from L Baisn

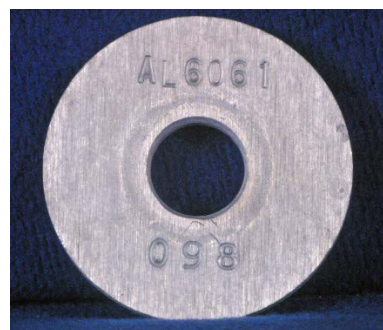


Upward/Downward



Creviced Surfaces

After cleaning in nitric acid solution



Al 6061 #098



Al 6061 #097

Al 6063 #128/Al 6063 #127

As-received from L Baisn

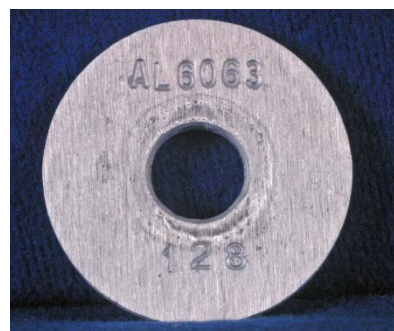


Upward/Downward

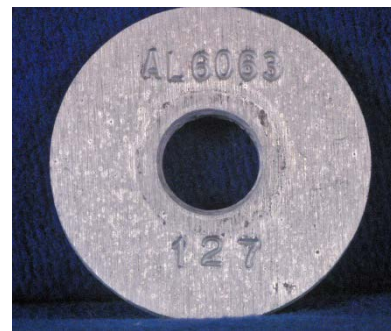


Creviced Surfaces

After cleaning in nitric acid solution



Al 6063 #128



Al 6063 #127

Al 6063 #126/Al 6063 #125

As-received from L Baisn

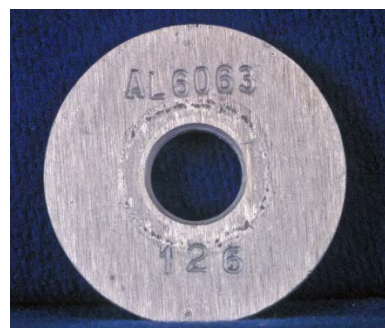


Upward/Downward



Creviced Surfaces

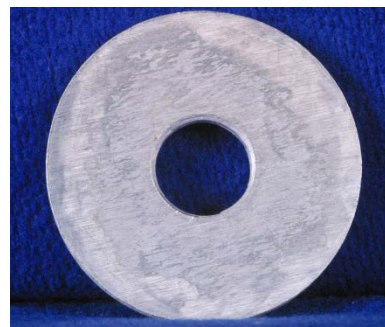
After cleaning in nitric acid solution



Al 6063 #126













Al 6063 #125













Appendix C Photographic Comparison of Surveillance Coupons from 2005 to 2014

Al 1100 Single Configuration

Year	Front Side – with numbers*	Back Side- without numbers
2005 6 years, inserted 1999		
2006 7 years, inserted 1999 Post sand filter event		
2008 9 years, inserted 1999		
2010 11 years, inserted 1999		
2014 15 years, inserted 1999		









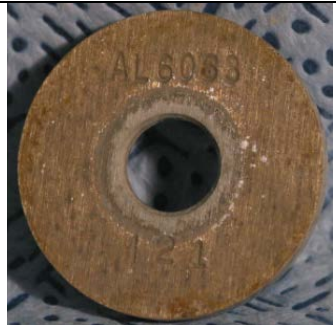

*Front side generally faced downward during exposure except 2006 which faced upward

Al 6061 Single Configuration

Year	Front Side – with numbers*	Back Side- without numbers
2004 8 years, inserted 1996 Pre sand filter event		
2006 7 years, inserted 1999 Post sand filter event		
2008 9 years, inserted 1999		
2010 11 years, inserted 1999		
2014 15 years, inserted 1999		




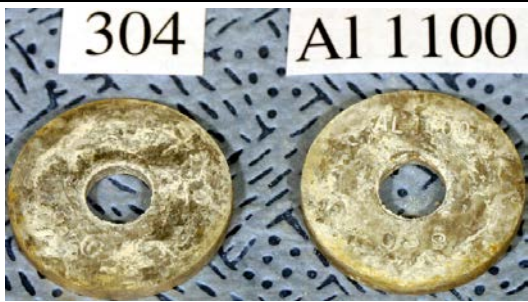






*Front side generally faced downward during exposure except 2006 which faced upward

Al 6063 Single Configuration

Year	Front Side – with numbers*	Back Side- without numbers
2004 8 years, inserted 1996 Pre sand filter event		
2006 7 years, inserted 1999 Post sand filter event		
2008 9 years, inserted 1999		
2010 11 years, inserted 1999		
2014 15 years, inserted 1999		

*Front side generally faced downward during exposure except 2006 which faced upward

Al 1100/304L Stainless Steel Galvanic Couple Configuration

Year	Non-mating sides*	Mating Sides
2005		
2006		
2008		
2010		
2014		

Appendix D XRD Scan of 2014 Aluminum Coupon

The scan below is same as shown in Figure 4-3.

